

Nitroxide/Substrate Weak Hydrogen Bonding: Attitude and Dynamics of Collisions in Solution

Jennifer L. Russ, Juan Gu, Kun-Hsiang Tsai, Tom Glass, James C. Duchamp, and Harry C. Dorn*

Contribution from the Department of Chemistry, Virginia Polytechnic Institute and State University, Blacksburg, Virginia, 24061, and Department of Chemistry, Emory and Henry College, Emory, Virginia 24327

Received June 29, 2006; E-mail: hdorn@vt.edu

Abstract: The study of intermolecular collisions and bonding interactions in solutions is of critical importance in understanding and predicting solute/solvent properties. Previous work has established that stable paramagnetic nitroxide molecules are excellent probes of intermolecular interactions for hydrogen bonding in polar solvents. In this study, ^1H , ^2H , ^{13}C , ^{15}N NMR and liquid/liquid intermolecular transfer dynamic nuclear polarization ($L^2\text{IT DNP}$) results are obtained for the paramagnetic probe molecule, TEMPO, interacting with the common aprotic and protic polar solvents, CH_3CN and CH_3CONH_2 , yielding a profile of both dipolar and scalar interactions. A significant scalar contact hyperfine is observed for the $\text{N}-\text{O}\cdots\text{H}-\text{C}$ interaction ($^{13}\text{CH}_3$ hyperfine, $a/h = 0.66$ MHz) in the $\text{CH}_3\text{CN}/\text{TEMPO}$ system, whereas the $\text{N}-\text{O}\cdots\text{H}-\text{C}$ and $\text{N}-\text{O}\cdots\text{H}-\text{N}$ interactions for the $\text{TEMPO}/\text{CH}_3\text{CONH}_2$ system yield $^{13}\text{CH}_3$ and ^{15}N hyperfine couplings of $a/h = 0.16$ and -0.50 MHz, respectively. The distance and attitude of the scalar interaction for the nitroxide hydrogen bonding at the methyl group in CH_3CN and the amino group in CH_3CONH_2 are computed using density functional theory (DFT), yielding good agreement with the experimental results. These results show that the hyperfine coupling provides a sensitive probe of weak hydrogen-bonding interactions in solution.

Introduction

Solution collisional dynamics and hydrogen bonding in solute/solvent systems employing nitroxide and other radicals have been an active area of interest for over 30 years.^{1–15} These previous studies have shown that stable nitroxide free radicals are excellent probe molecules that interact with weak protic solvent molecules providing insight into the short-lived complexes formed and can function as probes in biological studies.⁸ NMR contact shift studies have shown that the collision

interaction (or the very weak transient complex formed) between a paramagnetic probe nitroxide and a closed shell diamagnetic molecule can provide scalar contact shifts which depend on the Fermi contact electron/nucleus hyperfine coupling constant. In pioneering studies by Morishima, Grant, Kingsbury, and others, it was found that NMR contact shifts provide sensitive probes to study the distribution of unpaired electron spin on the diamagnetic solvent molecule perturbed by the interaction with these stable free radical molecules.^{9–15} These short-lived solvent/solute interactions during transient complex formation can involve weak hydrogen-bonding interactions that typically take place on a 10^{-8} to 10^{-11} s time scale (Figure 1).

Dynamic nuclear polarization (DNP) enhancements provide information characterizing the solute/solvent interactions and complement NMR scalar contact shift and relaxation studies. The combination of the NMR nuclear–electron relaxation rates and DNP enhancements yields collision parameters such as correlation times of the transient complex, the radical/nucleus distance of closest approach, and of critical importance, the relative magnitude of scalar and dipolar interactions during these intermolecular collisions.^{16–21} Recent studies have shown that

- (1) Stark, U.; Mullerwarmuth, W. *Ber. Bunsen-Ges. Phys. Chem.* **1990**, *94*, 168–172.
- (2) Borah, B.; Bates, R. D. *J. Chem. Phys.* **1981**, *74*, 1538–1545.
- (3) Bundfuss, K.; Meisegresch, K.; Mullerwarmuth, W. *J. Magn. Reson.* **1983**, *55*, 408–420.
- (4) Borah, B.; Bates, R. D. *Chem. Phys. Lett.* **1980**, *76*, 101–104.
- (5) Dally, E.; Müllerwarmuth, W. *Ber. Bunsen-Ges. Phys. Chem.* **1977**, *81*, 1133–1137.
- (6) Dally, E.; Müllerwarmuth, W. *Ber. Bunsen-Ges. Phys. Chem.* **1978**, *82*, 792–798.
- (7) Dally, E.; Müllerwarmuth, W. *Ber. Bunsen-Ges. Phys. Chem.* **1980**, *84*, 260–265.
- (8) Bennett, H. F.; Brown, R. D.; Keana, J. F. W.; Koenig, S. H.; Swartz, H. M. *Magn. Reson. Med.* **1990**, *14*, 40–55.
- (9) Morishima, I.; Kawakami, K.; Yonezawa, T.; Goto, K.; Imanari, M. *J. Am. Chem. Soc.* **1972**, *94*, 6555–6557.
- (10) Morishima, I.; Toyoda, K.; Yoshikawa, K.; Yonezawa, T. *J. Am. Chem. Soc.* **1973**, *95*, 8627–8630.
- (11) Morishima, I.; Ishihara, K.; Tomishima, T.; Inubushi, T.; Yonezawa, T. *J. Am. Chem. Soc.* **1975**, *97*, 2749–2756.
- (12) Qui, Z. W.; Grant, D. M.; Pugmire, R. J. *J. Am. Chem. Soc.* **1984**, *106*, 557–563.
- (13) Hu, J. Z.; Solum, M. S.; Wind, R. A.; Nilsson, B. L.; Peterson, M. A.; Pugmire, R. J.; Grant, D. M. *J. Phys. Chem. A* **2000**, *104*, 4413–4420.
- (14) Hu, J. Z.; Zhou, J. W.; Yang, B. L.; Li, L. Y.; Qiu, J. Q.; Ye, C. H.; Solum, M. S.; Wind, R. A.; Pugmire, R. J.; Grant, D. M. *Solid State Nucl. Magn. Reson.* **1997**, *8*, 129–137.
- (15) Draney, D.; Kingsbury, C. A. *J. Am. Chem. Soc.* **1981**, *103*, 1041–1047.

- (16) Dwek, R.; Richard, R.; Rex, E.; Taylor, D. *Ann. Rev. NMR Spectrosc.* **1969**, *2*, 293–344.
- (17) Potenza, J. *Adv. Mol. Relax. Processes* **1972**, *4*, 229–354. Hausser, K.; Stehlik, D. *Adv. Magn. Reson.* **1968**, *3*, 79.
- (18) Müller-Warmuth, W.; Meise-Gresch, K. *Adv. Magn. Reson.* **1983**, *11*, 1.
- (19) Bates, R. *Magn. Reson. Rev.* **1993**, *16*, 237.
- (20) Grucker, D.; Guiberteau, T.; Eclancher, B.; Chambron, J.; Chiarelli, R.; Rassat, A.; Subra, G.; Gallez, B. *J. Magn. Reson., Ser. B* **1995**, *106*, 101–109.

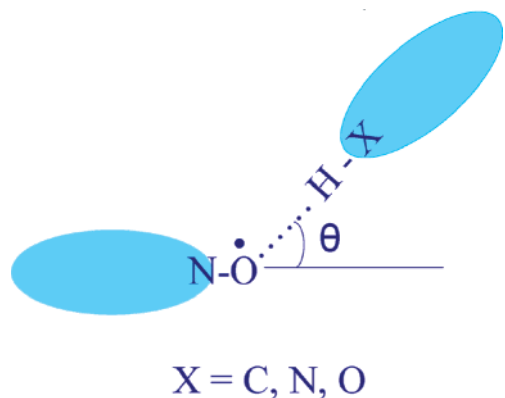


Figure 1. Nitroxide/substrate hydrogen-bonding interaction.

dynamic nuclear polarization (DNP) experiments can provide large enhancements of NMR signals for endogenous biological solutes.²² Our laboratory has previously described a liquid/liquid intermolecular flow transfer (L²IT) DNP technique that allows generation of the polarization at low magnetic fields (0.33 T) but transfer of the bolus to high magnetic fields for monitoring the greater chemical shift dispersion (¹H 200 MHz, 4.7 T).^{23–27} For NMR nuclei with low magnetogyric ratios (e.g., ¹³C), DNP enhancements may be very large, especially in the presence of a strong scalar interaction.^{23–26} The importance of scalar interactions at high magnetic fields was recently addressed by Griffin and co-workers.²⁸

More recently, computational tools that predict solution-state intra- and intermolecular parameters complement the corresponding solute/solvent experimental studies. For example, intramolecular paramagnetic NMR contact shift studies of metalloporphyrins and metalloproteins coupled with computational approaches provide a detailed picture of the hyperfine interaction.^{29–30} For intermolecular cases, computational studies have been reported for CH₃CN, a common polar aprotic solvent that complexes with water,³¹ methanol,³² and hydrogen chloride.³³ Rissi et al. performed calculations on the (CH₃CN···H₂O) complex using four different levels of theory.³¹ In this case, the reported interaction distances (H₃CCN···HOH) range from 2.036 to 2.106 Å, and the N–H–O angles are nearly linear (162.9–169.7°). Coussan and co-workers studied the CH₃CN interaction with methanol using DFT, and three stable orientations of the CH₃OH···CH₃CN complex were found.³² They found that the N–H and O–H intermolecular bond distances were in the 2–3 Å range, and the angles of interaction

range from approximately 115–180°. In another study, George and co-workers examined the CH₃CN···HCl system also using DFT, and the N–H bond distance was found to be ~2 Å, and the angle of the hydrogen-bond formation (N–H–Cl) is 180°.³³ Karplus and co-workers have studied the hydrogen-bonding interactions between simple dimers of *N*-methylacetamide (NMA) and the NMA/water complex.³⁴

Although there are numerous computational studies of the polar solvents, CH₃CN^{31–33} and CH₃CONH₂ (or molecules with an amide linkage),^{35–42} there is a paucity of computational hydrogen-bonding studies of nitroxides. A notable exception is the hybrid self-consistent Hartree–Fock and density functional (B3LYPA level) study by Barone and co-workers of the interaction of two water molecules with a nitroxide.⁴³ Another example is a computational study by Otsuka of the interaction of methanol and trichloromethane with the two nitroxyl radicals, DTBN (di-*tert*-butyl nitroxide) and DMNO (di-methyl nitroxide).⁴⁴ The latter study is one of the first to examine not only the dynamics and average distance of the interaction but also the distance and attitude of the solvent–nitroxide interaction.

In this paper, the CH₃CN/TEMPO and CH₃CONH₂/TEMPO systems were experimentally characterized by a combined NMR and L²IT DNP approach. The DFT computational studies were examined at different distances and attitudes of the complex interaction, and these were compared with the experimental hyperfine scalar couplings. The combined experimental/computational method provides a new approach to understanding the distance, attitude, dynamics, and energy of weak nitroxide solution interactions.

Experimental Section

In order to improve sensitivity of the NMR and DNP experiments, labeled samples were employed. Acetonitrile-¹⁵N and acetamide-¹⁵N were prepared from ¹⁵N-labeled ammonia as described previously.⁴⁵ Two ¹³C-labeled compounds, ¹³CH₃CONH₂ and CH₃¹³CONH₂, were synthesized using the starting commercial compounds ¹³CH₃COCl and CH₃¹³COCl (Aldrich Chemical Co.). 2,2,6,6-Tetramethyl-1-piperidinyloxy (TEMPO) and the other chemicals were purchased from Aldrich and used directly without further purification. The sample solutions of TEMPO/CH₃CN and TEMPO/CH₃CONH₂ were prepared and degassed by the freeze–pump–thaw method in carbon tetrachloride (CCl₄) and *p*-dioxane (C₄H₈O₂), respectively. Deuterated cyclohexane-*d*₁₂ was used as an internal lock. Separate sets of sample solutions with different concentrations of CH₃CN and CH₃CONH₂ were prepared to measure the complex formation constant *K*_c and hyperfine coupling constant, *a*, (see Supporting Information for details).

- (21) Odinstov, B. M.; Bedford, R. L.; Clarkson, R. B. *Phys. Chem. A* **1997**, *101*, 116–121.
 (22) Golman, K.; Ardenkjaer-Larsen, J. H.; Petersson, J. S.; Mansson, S.; Leunbach, I. B. *Proc. Natl. Acad. Sci. U.S.A.* **2003**, *100* (18), 10435–10439.
 (23) Tsai, K.; Dorn, H. C. *Appl. Magn. Reson.* **1990**, *1*, 231–254.
 (24) Dorn, H. C.; Glass, T. E.; Gitti, R.; Tsai, K. *Appl. Magn. Reson.* **1991**, *2*, 9–27.
 (25) Stevenson, S.; Glass, T.; Dorn, H. C. *Anal. Chem.* **1998**, *70*, 2623–2628.
 (26) Stevenson, S.; Dorn, H. C. *Anal. Chem.* **1994**, *66*, 2993–2999.
 (27) Dorn, H. C.; Gu, J.; Bethune, D. S.; Johnson, R. D.; Yannoni, N. S. *Phys. Chem. Lett.* **1993**, *203*, 549–554.
 (28) Loening, N. M.; Rosay, M.; Weis, V.; Griffin, R. G. *J. Am. Chem. Soc.* **2002**, *124*, 8808–8809.
 (29) Mao, J. H.; Zhang, Y.; Oldfield, E. *J. Am. Chem. Soc.* **2002**, *124*, 13911–13920.
 (30) Wilkens, S. J.; Xia, B.; Weinhold, F.; Markley, J. L.; Westler, W. M., J. *Am. Chem. Soc.* **1998**, *120*, 4806–4814.
 (31) Rissi, E.; Fileti, E.; Canuto, S. *Theor. Chem. Acc.* **2003**, *110*, 360–366.
 (32) Coussan, S.; Bouteiller, Y.; Perchard, J.; Brenner, V.; Millie, P.; Zheng, W.; Talbot, F. *J. Chem. Phys.* **1999**, *110*, 10046–10057.
 (33) George, W.; Jones, B.; Lewis, R.; Price, J. *Phys. Chem. Chem. Phys.* **2000**, *2*, 4910–4917.

- (34) Buck, M.; Karplus, M. *J. Phys. Chem. B* **2001**, *105*, 11000–11015.
 (35) Kim, K.-Y.; Lee, H.-J.; Karpfen, A.; Park, J.; Yoon, C.-J.; Choi, Y.-S. *Phys. Chem. Chem. Phys.* **2001**, *3*, 1973–1978.
 (36) Aquino, A.; Tunega, D.; Habershauer, G.; Gerzabek, M.; Lischka, H. *J. Phys. Chem. A* **2002**, *106*, 1862–1871.
 (37) Watson, T.; Hirst, J. *Phys. Chem. Chem. Phys.* **2004**, *6*, 998–1005.
 (38) Kaminski, G.; Maple, J.; Murphy, R.; Braden, D.; Friesner, R. *J. Chem. Theor. Comput.* **2005**, *1*, 248–254.
 (39) Kim, J.; Lee, H.-J.; Kim, E.-J.; Jung, H.; Choi, Y.-S.; Park, J.; Yoon, C.-J. *J. Phys. Chem. A* **2004**, *108*, 921–927.
 (40) Johnson, M.; Prager, M.; Grimm, H.; Neumann, M.; Kearley, G.; Wilson, C. *Chem. Phys.* **1999**, *244*, 49–66.
 (41) Kubelka, J.; Keiderling, T. *J. Phys. Chem. A* **2001**, *105*, 10922–10928.
 (42) Trikoupi, M.; Burgers, P.; Ruttink, P.; Terlouw, J. *Int. J. Mass Spectrom. Ion Processes* **2001**, *210/211*, 489–501.
 (43) Barone, V.; Bencini, A.; Cossi, M.; Di Matteo, A.; Mattisini, M.; Mattesini, M.; Totti, F. *J. Am. Chem. Soc.* **1998**, *120*, 7069–7078.
 (44) Otsuka, T.; Motozaki, W.; Nishikawa, K.; Endo, K. *J. Mol. Struct.* **2002**, *615*, 147–151.
 (45) Morgan, D.; Dorn, H. C. *J. Labelled Compd. Radiopharm.* **1991**, *29*, 777–779.

The radical-induced ^{13}C and ^{15}N chemical shifts were measured by using procedures described in the literature.^{9–11,27} The ^{13}C and ^{15}N spin–lattice relaxation time measurements (T_1) were performed utilizing Jeol FX-80, FX-200, and Varian 400 NMR spectrometers and were measured by an inversion recovery method using a $180^\circ\text{--}\tau\text{--}90^\circ$ pulse sequence. The ^1H spin–lattice relaxation time was measured and used to obtain the radical-induced relaxation rate $(1/T_1)_{\text{rad}}$. The ^{13}C and ^{15}N spin–spin relaxation times T_2 were obtained from line broadening measurements of the respective NMR signals in the presence of TEMPO.

The instrument used in the L²IT DNP experiments was described previously and is briefly described below.^{23–24} A variable electromagnet (0.33 T) is placed orthogonally under a 4.7 T superconducting magnet at a distance of 1.2 m from the centers of the respective magnet fields. A ceramic flow sample tube was placed in a microwave TE₁₀₂ cavity of a modified Varian E-3 EPR spectrometer. The microwave frequency was generated in a klystron of a Bruker microwave bridge and amplified by a Varian “K” series TWT amplifier, and the microwave power was adjusted by an attenuator to the range of 1–16 W. In this way, the sample is polarized at a low magnetic field (0.33 T) and then is flow transferred to a high magnetic field for detection (4.7 T). To determine the DNP enhancement in the flow system the observed NMR signals, in the presence of low magnetic field with and without the microwave power, were measured as a function of flow rates ranging from 2 to 9 mL/min. The ultimate ^1H , ^2H , ^{13}C , and ^{15}N DNP enhancements were obtained using the experimental protocol described previously.^{23–27}

The geometry of the TEMPO structure was obtained by performing an optimization calculation on the monoclinic crystal structure of TEMPO.⁴⁶ The geometry of the TEMPO structure acquired from the optimization calculation was used for all acetonitrile/TEMPO and acetamide/TEMPO calculations. The structures of acetonitrile and acetamide were also optimized using the UB3LYP level of theory and the basis set previously mentioned.

The DFT calculations were performed using the Gaussian 98 and Gaussian 03 programs.^{47–48} The UB3LYP level of theory^{49–50} with the Chipman DZP + Diffuse (with the first d-type polarization function removed for C, N, and O) basis set were used.⁵¹ The computations were performed on a SGI ALTIX 3700 Supercluster Computer at Virginia Tech. The Supercluster consists of 16 1.3-GHz Itanium processors each allocated of 3 MB of cache, 24 GB of memory, 36 GB of internal disk storage, and 500 GB of RAID disk storage. Molecular orbital diagrams were prepared with Gaussview⁵² (for details on the geometries and other computational details see SI).

Results and Discussion

Nitroxide/Substrate Dynamic Nuclear Polarization (DNP).

The nitroxide/substrate collision and/or weak complex formation in solution may be conveniently monitored utilizing DNP. For DNP, the time-dependent Overhauser enhancement, A , may be expressed in the simplified form given^{17–19} in eq 1, where γ_s and γ_I are the magnetogyric ratios for the nuclear and electron

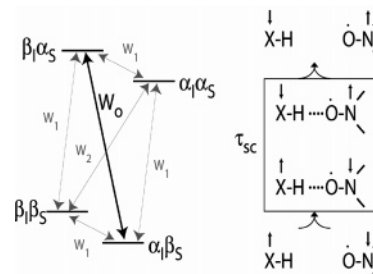


Figure 2. Energy level diagram with transition probabilities for a dominant scalar (W_0) interaction. In a magnetic field, the β_s spin state of the nitroxide ($\text{N}\text{--}\text{O}$) and the nuclear spin, α_I of the X nuclide (e.g., ^{13}C , $\gamma_I > 0$) are more stable. The spin orientations (right side) for the X nuclide will be reversed for ^{15}N , $\gamma_I < 0$. The diagram (right side) assumes a direct $\text{N}\text{--}\text{O}$ interaction with nuclide X.

spins, respectively, and the coupling (Δ) and leakage (f) factors are defined in terms of the transition probabilities W_2^{D} , W_0^{D} , W_1^{D} , etc. for the nucleus/electron interaction in eqs 2 and 3.

$$A = \frac{A_z - A_0}{A_0} = \frac{-\rho f s |\gamma_s|}{\gamma_I} \quad (1)$$

$$\rho = \frac{W_2^{\text{D}} - W_0^{\text{D}} - W_0^{\text{SC}}}{W_2^{\text{D}} + W_0^{\text{D}} + W_0^{\text{SC}} + 2W_1^{\text{D}}} \quad (2)$$

$$f = \frac{W_0^{\text{D}} + 2W_1^{\text{D}} + W_2^{\text{D}} + W_0^{\text{SC}}}{W_0^{\text{D}} + 2W_1^{\text{D}} + W_2^{\text{D}} + W_0^{\text{SC}} + W_{10}} \quad (3)$$

$$f = 1 - \frac{T_{1n}}{T_{1no}} \quad (4)$$

The critical time-dependent DNP parameter is the coupling factor (ρ) which is a sensitive measure of the relative scalar/dipolar strength. The value of ρ ranges from a pure scalar interaction ($W_0^{\text{D}}:W_1^{\text{D}}:W_2^{\text{D}} = 0$, $\rho = -1$) to a dominant dipolar interaction, $W_0^{\text{SC}} \approx 0$. The latter dipolar-dominated enhancement has an ultimate limiting value of +0.5 in the extreme narrowing limit $\omega_s \tau_c \ll 1$ ($W_0^{\text{D}}:W_1^{\text{D}}:W_2^{\text{D}} = 2:3:12$). The energy diagram and interacting spins are illustrated in Figure 2 for a dominant scalar intermolecular interaction of an unpaired nitroxide electron spin with spin states, α_s and β_s with nuclear spins, α_I and β_I . The nuclear spin–lattice relaxation rates in the presence and absence of a free radical are given by $(T_{1n})^{-1} - (T_{1no})^{-1} = (W_0^{\text{D}} + 2W_1^{\text{D}} + W_2^{\text{D}} + W_0^{\text{SC}})$ and $(T_{1no})^{-1} = W_{10}$, respectively. The leakage factor, f , is determined from spin–lattice relaxation time measurements in the presence and the absence of the free radical, TEMPO. The electron spin saturation factor, s , is given by

$$s = \frac{S_0 - \bar{S}_Z}{S_0} \quad (5)$$

where \bar{S}_Z is defined in eq 6 as

$$\bar{S}_Z = \frac{S_0}{1 + \alpha B_{1s}^2 T_{1s} T_{2s}} \quad (6)$$

where T_{1s} and T_{2s} are the electron spin–lattice and spin–spin relaxation times, respectively. The electron spin saturation factor

(46) Bordeaux, D.; Lajzerowicz-Bonneteau, J.; Briere, R.; Lemaire, H.; Rassat, A. *Org. Magn. Reson.* **1973**, *5*, 47–52.

(47) Frisch, M. J.; et al. *Gaussian 98*; Gaussian, Inc.: Pittsburgh, PA, 2001.

(48) Frisch, M. J.; et al. *Gaussian 03*, Revision C.02; Gaussian, Inc.: Wallingford, CT, 2004.

(49) Becke, A. J. *Chem. Phys.* **1993**, *98*, 5648–5652.

(50) Lee, C.; Yang, W.; Parr, R. *Phys. Rev. B* **1988**, *37*, 785–789.

(51) Basis sets were obtained from the Extensible Computational Chemistry Environment Basis Set, Database V, as developed and distributed by the Molecular Science Computing Facility, Environmental and Molecular Sciences Laboratory which is part of the Pacific Northwest Laboratory, P.O. Box 999, Richland, Washington 99352, U.S.A., and funded by the U.S. Department of Energy. The Pacific Northwest Laboratory is a multi-program laboratory operated by Battelle Memorial Institute for the U.S. Department of Energy under contract DE-AC06-76RLO 1830. Contact Karen Schuchardt for further information.

(52) Dennington, R.; Keith, T.; Millam, J.; Eppinnett, K.; Hovell, W. L.; Gilliland, R. *GaussView*, 3.09; Semichem, Inc.: Shawnee Mission, KS, 2003.

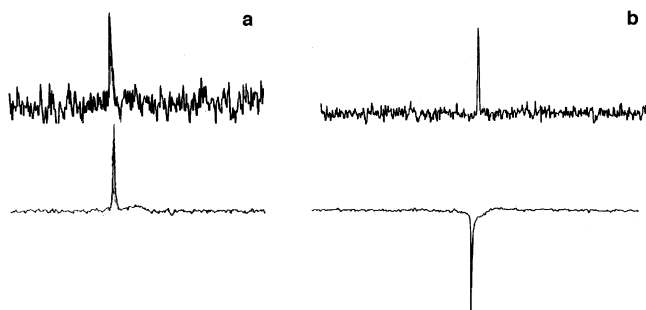


Figure 3. NMR (top) and DNP enhanced (bottom) spectra of $\text{CH}_3\text{CN}/\text{TEMPO}$ (a) and $\text{CH}_3\text{CONH}_2/\text{TEMPO}$ (b). (a) ^{15}N NMR spectrum (120 scans, 2460 s) and DNP enhanced spectrum (120 scans, 156 s). (b) ^{15}N NMR spectrum (1920 scans, 39 360 s) and DNP enhanced spectrum (120 scans, 180 s).

Table 1. DNP^a Results for the $\text{CH}_3\text{CN}/\text{TEMPO}$ and $\text{CH}_3\text{CONH}_2/\text{TEMPO}$ Systems

system	nucleus	<i>f</i>	<i>s</i>	A_∞^b	<i>r</i>	τ_r (ps)
$\text{CH}_3\text{CN}/\text{TEMPO}$	$-\text{C}^2\text{H}_3$	0.69	0.79	-1100 ± 100^b	0.26	50
	$-\text{C}^1\text{H}_3$	0.91	0.93	-160 ± 20	0.24	52
	$^{-13}\text{CH}_3$	0.71	0.75	$+520 \pm 100$	-0.20	—
	^{-13}CN	0.97	0.65	-620 ± 120	0.24	52
	$-\text{C}^{15}\text{N}$	0.97	0.50	$+520 \pm 100$	0.08	—
$\text{CH}_3\text{CONH}_2 / \text{TEMPO}$	$^{-13}\text{CH}_3$	0.94	0.37	60 ± 30^c	0.02	—
	^{-13}CO	0.97	0.46	-310 ± 30	0.12	62
	$^{-15}\text{NH}_2$	0.73	0.83	-2310 ± 460	-0.35	—

^a For the ^{13}C DNP and ^{15}N DNP experiments, inverse gated ^1H decoupling was employed to minimize any residual nuclear Overhauser effects. All data were obtained at room temperature. Concentrations are 1.34 M $\text{CH}_3\text{CN}/\text{CCl}_4/0.1$ M TEMPO and 0.4 M $\text{CH}_3\text{CONH}_2/\text{dioxane}/0.1$ M TEMPO. ^b DNP enhancements at low magnetic field (0.33 T) were monitored at high magnetic field (4.7 T). ^c Standard deviations were obtained from regression analysis.

Table 2. Radical-Induced Methyl ^1H Relaxation Time^a of $\text{CH}_3\text{CN}/\text{TEMPO}^b$ and $\text{CH}_3\text{CONH}_2/\text{TEMPO}^c$ Solution as a Function of Magnetic Field

magnetic field (T)	1.9	4.7	9.4
T_1 (s) (CH_3CN)	0.051 ± 0.003	0.049 ± 0.003	0.051 ± 0.000
T_1 (s) (CH_3CONH_2)	0.06 ± 0.03	0.05 ± 0.01	0.054 ± 0.000

^a All measurements were made at room temperature. ^b 1.34 M CH_3CN in CCl_4 with 0.1 M TEMPO solution. ^c 0.4 M CH_3CONH_2 in $\text{C}_4\text{H}_8\text{O}_2$ with 0.1 M TEMPO solution.

is experimentally evaluated from a plot of the inverse observed enhancement versus the microwave power applied to the electron spin system. The DNP enhancement factor for flowing systems has been obtained using an experimental apparatus previously reported by our laboratory.^{23–27} In a flow transfer DNP experiment, the nuclear spin system is polarized in a low magnetic field (0.33 T) and rapidly transferred (via flow) to a high, monitoring magnetic field, 4.7 T. We have previously reported a model²³ for the low-to-high magnetic field transfer experiment which provides a method for determining the absolute enhancement, A_∞ .

Representative ^{15}N DNP spectra are shown in Figure 3, and the ultimate ^1H , ^2H , ^{15}N , and ^{13}C DNP enhancements, A_∞ for the $\text{CH}_3\text{CN}/\text{TEMPO}$ and $\text{CH}_3\text{CONH}_2/\text{TEMPO}$ systems are presented in Table 1. In the $\text{CH}_3\text{CN}/\text{TEMPO}$ system, the ^{13}C DNP enhancement for the peak assigned to the methyl carbon exhibits a large scalar enhancement in comparison with the dipolar-dominated enhancements for the cyano sp-hybridized carbon, whereas a mixed interaction for the ^{15}N cyano nitrogen is suggested by the significant, but reduced, ρ value of 0.08.

This result agrees with work from Grant's group in which nitroxide-induced ^{13}C NMR chemical shift studies of aromatic nitrogen compounds suggest that the N–O group in TEMPO orients away from aromatic sp^2 nitrogen atoms (without attached hydrogen atoms).¹² This result is also consistent with a significantly larger hyperfine coupling obtained in the current study for the NMR contact shifts for the $\text{CH}_3\text{CN}/\text{TEMPO}$ system, *vide infra*. As shown in Table 1, the methyl hydrogen atoms (^1H , ^2H) and the nitrile sp-hybridized ^{13}C carbon have similar ρ values and are dominated by a dipolar interaction. Assuming a rotationally modulated mechanism dominates this dipolar interaction, the corresponding rotational correlation time (τ_r) is estimated from the expression for exclusive rotational dipolar diffusion^{17–19}

$$\rho_D^r = \frac{1}{1.4 + 0.6 \left[\frac{J_D^r(\omega_I)}{J_D^r(\omega_S)} \right]} \quad (7)$$

$$J_D^r(\omega) = \left(\frac{1}{2\pi r^6} \right) \left[\frac{\tau_r}{1 + \omega^2 \tau_r^2} \right] \quad (8)$$

where r is the nucleus/electron distance in the complex. This leads to values of 50–52 ps for the rotational correlation time for the $\text{CH}_3\text{CN}/\text{TEMPO}$ system.

In contrast with $\text{CH}_3\text{CN}/\text{TEMPO}$, the $\text{CH}_3\text{CONH}_2/\text{TEMPO}$ system exhibits a large, scalar-dominated ^{15}N DNP enhancement and a very small ^{13}C dipolar DNP enhancement for the methyl carbon (Figure 3 and Table 1). Although earlier ^{15}N DNP results have been reported by the groups of Grant, Wind, and Griffin, the large scalar-dominated Overhauser enhancement for the $\text{CH}_3\text{-CONH}_2/\text{TEMPO}$ system is the first reported for solution-state studies.^{53–54} The results are consistent with the model of weak hydrogen-bond formation where the TEMPO radical tends to form a hydrogen-bonded transient complex with the N–H group between the amino proton and the N–O group. This interaction yields a relatively large scalar enhancement at the amino nitrogen nucleus. The small negative ($\rho \approx 0$) ^{13}C DNP enhancement observed for the methyl carbon suggests a mixed scalar and dipolar interaction at this field strength. In contrast with the $\text{CH}_3\text{CN}/\text{TEMPO}$ system, this system exhibits a diminished C–H bond interaction for the methyl group. For this case, only the carbonyl carbon is clearly dominated by a dipolar interaction, assuming a rotational model leads to a slightly longer value (62 ps) for the rotational correlation time. The observation of exclusively dipolar enhancements for the carbonyl group is consistent with DNP results for other small molecules containing carbonyl groups (e.g., acetaldehyde, acetone, etc.).⁵⁵

Nitroxide/Substrate NMR Relaxation. The importance of NMR spin–lattice, T_1 , and spin–spin, T_2 , dipolar and scalar nucleus/electron relaxation rates to characterize intermolecular interactions in solution has been described over the last five decades.^{56–63} The observed nuclear relaxation rate is given by

- (53) Hu, J. Z.; Solum, M. S.; Wind, R. A.; Nilsson, B. L.; Peterson, M. A.; Pugmire, R. J.; Grant, D. M. *J. Phys. Chem. A* **2000**, *104*, 4413–4420.
 (54) Hall, D. A.; Maus, D. C.; Gerfen, G. J.; Inati, S. J.; Becerra, L. R.; Dahlquist, F. W.; Griffin, R. G. *Science* **1997**, *276*, 930.
 (55) Sun, Z. Ph.D. Thesis, Virginia Tech, Blacksburg, VA, 1996.
 (56) Abragam, A. *The Principles of Nuclear Magnetism*; Clarendon: Oxford, England, 1961.
 (57) Bloembergen, N.; Purcell, E.; Pound, R. *Phys. Rev.* **1948**, *73*, 679–712.

the sum of the radical-induced dipolar and scalar contribution as well as the nucleus/nucleus interactions ($1/T_{10}$) as

$$\left(\frac{1}{T_1}\right)_{\text{obs}} = \left(\frac{1}{T_1}\right)_{\text{rad}} + \left(\frac{1}{T_{10}}\right) = W_0^{\text{D}} + 2W_2^{\text{D}} + W_0^{\text{D}} + W_0^{\text{SC}} + 2W_{10} \quad (9)$$

The radical-induced relaxation rate $(1/T_1)_{\text{rad}}$ was obtained by subtracting $1/T_{10}$ from the observed relaxation rate $(1/T_1)_{\text{obs}}$ (eq 9). In principle, dipolar interactions between the electrons and the nuclei may be modulated by either translational or rotational diffusion motion of the molecules. In the case of weak nitroxide/substrate complex formation, the scalar interaction is also a possible relaxation mechanism. Various models have been proposed for the scalar interaction including a so-called “sticking model”⁶¹ and a diffusion model.⁵⁸ The exact form of the transition probabilities, W_i , depend on the model chosen for modulation. When the sample and radical molecules form a transient complex, the dipolar coupling may be modulated by rotational tumbling of the associated species, and the scalar coupling may be modulated by the “on–off” mechanism of the complex formation. When the conditions $\omega_S\tau_r \gg \omega_I\tau_r$ and $\omega_I\tau_r \ll 1$ are satisfied and $J(\omega_S \pm \omega_I) \approx J(\omega_S)$, the radical-induced relaxation rates are given as

$$\left(\frac{1}{T_1}\right)_{\text{rad}} = \frac{1}{10} \left(\frac{\mu_0}{4\pi}\right)^2 \frac{\gamma_I^2 \gamma_S^2 \pi^2 \chi}{r^6} \left(\frac{3\tau_c}{1 + \omega_I^2 \tau_c^2} + \frac{7\tau_c}{1 + \omega_I^2 \tau_c^2} \right) + \frac{1}{2} \left(\frac{a}{\hbar}\right)^2 \chi \left(\frac{\tau_{\text{SC}}}{1 + \omega_I^2 \tau_{\text{SC}}^2} \right) \quad (10)$$

$$\left(\frac{1}{T_2}\right)_{\text{rad}} = \frac{1}{20} \left(\frac{\mu_0}{4\pi}\right)^2 \frac{\gamma_I^2 \gamma_S^2 \pi^2 \chi}{r^6} \left(4\tau_c \frac{3\tau_c}{1 + \omega_I^2 \tau_c^2} + \frac{13\tau_c}{1 + \omega_I^2 \tau_c^2} \right) + \frac{1}{4} \left(\frac{a}{\hbar}\right)^2 \chi \left(\tau_{\text{SC}} + \frac{\tau_{\text{SC}}}{1 + \omega_S^2 \tau_{\text{SC}}^2} \right) \quad (11)$$

where τ_c is the more general form of the correlation time including translation and rotational motion (see eqs 7 and 8 for exclusive rotation), τ_{SC} is the scalar correlation time, r is the average pair radius for the rotating adduct, and μ_0 is the permeability constant. χ is the fraction of time the nuclear spin is in the paramagnetic environment and may be considered as the fraction of associated radical–receptor complex in the fast exchange case.

Almost all previous ^1H NMR and DNP studies indicate that the dipolar interactions dominate between hydrogen nuclei and the unpaired electron spin regardless of the free radical or the solvent employed. However, a notable exception has been reported by Bates in a nitroxide/trifluoroacetic system.^{19,62} In the current study, the ^1H DNP results for the $\text{CH}_3\text{CN}/\text{TEMPO}$ system presented in Table 1 are consistent with the dominance of the dipolar interaction. The spin–lattice relaxation times for the methyl protons measured at different magnetic field strengths are presented in Table 2. By subtracting $(1/T_{10})$ from $(1/T_1)_{\text{obs}}$

at a given field strength, $(1/T_1)_{\text{rad}}$ was obtained. The results show that the relaxation times of the $-\text{CH}_3$ protons in both systems reach a plateau in the range of observed frequencies.

The observation of a pronounced plateau in the data from 1.9 to 9.4 T is strong evidence that the relaxation is dominated by a rotationally driven dipolar coupling of the two spins.² Assuming that the complex undergoes isotropic rotational diffusion and the nitroxide radical is bound in a 1:1 complex to a solvent molecule, $(1/T_1)_{\text{rad}}$ is given by

$$\left(\frac{1}{T_1}\right)_{\text{rad}} = \frac{1}{10} \left(\frac{\mu_0}{4\pi}\right)^2 \frac{\gamma_I^2 \gamma_S^2 \pi^2 \chi}{r^6} \left(\frac{3\tau_c}{1 + \omega_I^2 \tau_c^2} + \frac{7\tau_c}{1 + \omega_I^2 \tau_c^2} \right) \quad (12)$$

where χ is the fraction of the complex which is taken from the chemical contact shift measurement (*vide infra*). The radical-induced relaxation rates at different magnetic frequencies were fitted to eq 12 using a nonlinear regression program, giving rotational correlation times for the $\text{CH}_3\text{CN}/\text{TEMPO}$ and $\text{CH}_3\text{-CONH}_2/\text{TEMPO}$ system of $\tau_r = 30$ and 35 ps respectively. These values are ~60% lower than the values directly obtained from the DNP measurements, but both approaches indicate a slightly longer rotational correlation time for the $\text{CH}_3\text{CONH}_2/\text{TEMPO}$ system. Using this range of correlation times (e.g., 30–52 ps for the $\text{CH}_3\text{CN}/\text{TEMPO}$) and a range of χ values, eq 11 allows an estimate of r (i.e., the distance between the hydrogen and the radical delocalized on the nitroxyl group). In this manner, we estimate a range of values, 0.30–0.45 nm, for the $\text{CH}_3\text{CN}/\text{TEMPO}$ system, whereas the $\text{CH}_3\text{CONH}_2/\text{TEMPO}$ system values are slightly longer, 0.32–0.48 nm.

It is also possible to estimate the correlation time for the scalar hyperfine interaction correlation time (τ_{SC}) with a combination of the rotational model for the dipolar interaction and the sticking model for the scalar interaction based on eqs 10 and 11. Under the condition of $\omega_I^2 \tau^2 \ll 1$ and $\omega_S^2 \tau \gg 1$, the difference between $(1/T_1)_{\text{rad}}$ and $(1/T_2)_{\text{rad}}$ is given as

$$\left(\frac{1}{T_2}\right)_{\text{rad}} - \left(\frac{1}{T_1}\right)_{\text{rad}} = \frac{1}{20} \left(\frac{\mu_0}{4\pi}\right)^2 \frac{\gamma_I^2 \gamma_S^2 \pi^2 \chi}{r^6} + \frac{1}{4} \left(\frac{a}{\hbar}\right)^2 \chi \tau_{\text{SC}} \quad (13)$$

Therefore, the scalar correlation time τ_{SC} may be determined on the basis of eq 13 since all other parameters are known. In this study the ^{13}C relaxation rates, $1/T_1$ and $1/T_2$, of the methyl carbon were measured at a fixed magnetic field (9.4 T). The value of the hyperfine coupling constant a and the mole fraction χ are obtained from the NMR contact shift measurement (*vide infra*). Of particular interest in the current study is the Fermi interaction and corresponding hyperfine coupling constant (a) which is given by

$$a = (8\pi/3) \gamma_S \gamma_I \hbar^2 |\psi(0)|^2 \quad (14)$$

where $|\psi(0)|^2$ represents the unpaired spin density at the nucleus X (see Figure 2). The rotational correlation time τ_r was obtained from the ^1H relaxation frequency-dependent measurement previously described. The value of the closest distance between the unpaired electron and the methyl carbon is estimated from the sum of r and the C–H bond length, giving values of 0.40–0.55 nm for the $\text{CH}_3\text{CN}/\text{TEMPO}$ system. In this way a scalar correlation time of ~85 ps is estimated for the $\text{CH}_3\text{CN}/\text{TEMPO}$ system. A value 2–3 times longer than the rotational correlation

(58) Hubbard, P. *Proc. R. Soc. London A* **1966**, 291, 537–555.

(59) Poindexter, E.; Caplan, P.; Wagner, B.; Bates, R., Jr. *J. Chem. Phys.* **1974**, 61, 3821–3827.

(60) Solomon, I. *Phys. Rev.* **1955**, 99, 559–565.

(61) Solomon, I. *J. Chem. Phys.* **1956**, 25, 261–266.

(62) Al-Bala'a, I.; Bates, R. D. *J. Magn. Reson.* **1988**, 78, 271–280.

(63) Pfeifer, H. *Ann. Phys.* **1961**, 463, 1–8.

Table 3. ^{13}C and ^{15}N Contact Shifts and Hyperfine Constants (a) for the Acetamide/TEMPO and Acetonitrile/TEMPO Systems

$\text{CH}_3\text{CONH}_2/\text{TEMPO}$ system				$\text{CH}_3\text{CN}/\text{TEMPO}$ system			
group	Δ_0 (ppm)	a/h (MHz)	K_c	group	Δ_0 (ppm)	a/h (MHz)	K_c
$^{-13}\text{CH}_3$	$17^a \pm 1$	0.16 ± 0.01	0.48 ± 0.04	$^{-13}\text{CH}_3$	$70^a \pm 4$	0.66 ± 0.04	0.8 ± 0.08
$^{-13}\text{CONH}_2$	$-1^a \pm 2$	-0.01 ± 0.02		^{-13}CN	$0^a \pm 2$	0	
$^{-15}\text{NH}_2$	130 ± 10	-0.5 ± 0.04	0.48 ± 0.05	^{-15}N	22 ± 4	-0.08 ± 0.02	0.6 ± 0.1

^a The values are calculated from chemical shifts versus the concentration plot and corrected with the internal reference cyclohexane, $\Delta_0 = 4.0$ ppm over the concentration of 0.4–2.0 M TEMPO.

time appears reasonable for the lifetime of the weak C–H hydrogen-bond complex. In the case of labile complex formation, the scalar correlation time is defined as the sum of two terms, τ_h the life-time of the complex and τ_S the electron spin–lattice relaxation time. We assume τ_S is longer than τ_h for nitroxide radicals.⁶³

In order to obtain the scalar correlation time for the $\text{CH}_3\text{CONH}_2/\text{TEMPO}$ system, the ^{15}N relaxation rates, $1/T_1$ and $1/T_2$, have been measured at the fixed magnetic field (9.4 T). The hyperfine constant, a , and the molar fraction of the complex, χ , are taken from the contact shift measurement, and the correlation time τ_c is taken from the proton relaxation measurement. The scalar correlation time $\tau_{SC} \approx 120$ ps is estimated for the $\text{CH}_3\text{CONH}_2/\text{TEMPO}$ system using the same method as for the $\text{CH}_3\text{CN}/\text{TEMPO}$ system. The considerably longer scalar correlation time in the $\text{CH}_3\text{CONH}_2/\text{TEMPO}$ system is also consistent with a longer rotational correlation time and a significantly larger hyperfine coupling derived from the ^{15}N NMR contact shift measurements below.

Nitroxide/Substrate NMR Contact Shifts. As previously indicated, NMR contact shifts provide an alternative approach for monitoring the collision and/or very weak transient complex formed between a paramagnetic nitroxide and a closed shell diamagnetic molecule. These Fermi contact chemical shifts provide a well-established approach to measure the association equilibria between the substrate molecule and nitroxide as well as the corresponding hyperfine coupling constant at the substrate nuclide of interest.^{64,65} In order to determine the complex formation constant K_c and limiting contact shift of the complex Δ_0 , the experimental data have been analyzed using eq 14.

$$\frac{C_R}{\Delta} = \frac{1}{K_c \Delta_0} + \frac{C_0}{\Delta_0} \quad (15)$$

The radical-induced contact shift, Δ , will depend on the concentration of the diamagnetic molecule C_0 , and the radical concentration C_R .^{5–7} Therefore, Δ_0 and K_c may be determined from the slope and the intercept of the plot C_R/Δ versus C_0 . The hyperfine coupling constant a is obtained from the Fermi contact shift by the relation^{64–65}

$$\Delta_0 = -\frac{\gamma_S a}{\gamma_I 4kT} \quad (16)$$

where γ_S is the gyromagnetic ratio of the electron and γ_I is the gyromagnetic ratio of the nucleus. After obtaining the limiting contact shifts Δ_0 , the hyperfine coupling constants a/h are calculated on the basis of eq 15. The paramagnetic-induced contact shifts for ^{15}N , $^{13}\text{CH}_3$, and ^{13}CN for the $\text{CH}_3\text{CN}/\text{TEMPO}$

system were measured by varying the concentration of CH_3CN from 0.4 to 2.0 M in TEMPO, and the results are presented in Table 3. Consistent with the DNP results (*vide supra*), a relatively large scalar contact interaction ($a/h = -0.50$ MHz) is obtained at the nitrogen ^{15}N -amino group in the $\text{CH}_3\text{CONH}_2/\text{TEMPO}$ system which contrasts with the negligible scalar interaction at the nitrogen ^{15}N -cyano group for the $\text{CH}_3\text{CN}/\text{TEMPO}$ system. A large scalar interaction is also observed at the ^{13}C -methyl carbon ($a/h = 0.66$ MHz) for the $\text{CH}_3\text{CN}/\text{TEMPO}$ system, and a significantly reduced scalar interaction is present at ^{13}C -methyl group in the $\text{CH}_3\text{CONH}_2/\text{TEMPO}$ system. For the latter methyl ($-\text{CH}_3$) group, the DNP results indicate a very small dipolar enhancement ($A = -60$, see Table 1), but this value represents nearly equal dipolar and scalar contributions to the DNP enhancement at this frequency. A better measure of this interaction is the contact shift data (Table 3) which indicates a reduced, but still significant, hyperfine coupling constant ($a/h = 0.16$ MHz). The equilibrium constants, K_c , measured for the $\text{CH}_3\text{CN}/\text{TEMPO}$ and $\text{CH}_3\text{CONH}_2/\text{TEMPO}$ systems are consistent with values reported for a nitroxide/aniline system.¹ It is also interesting to note that both the carbonyl carbon of acetamide and the cyano carbon of acetonitrile have negligible scalar interactions with TEMPO. This is consistent with unfavorable electrostatic interactions of these groups with the polar nitroxide (N–O) bond and with the assumption of a dominant dipolar interaction that was observed above for the DNP results.

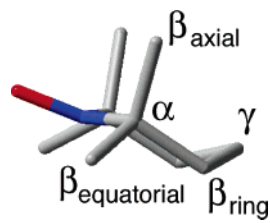
Hyperfine Interactions: Computational Approach. It is well recognized that Brownian motion leads to many different types of collisions in a solute/solvent system. As one example, the previously described $\text{CH}_3\text{CN}/\text{TEMPO}$ system provides correlation times that are nearly equal at different sites in the molecule (e.g., methyl hydrogens and cyano carbons) where nonspecific dipolar interactions are observed. In contrast, other collisions exhibit weak hydrogen-bonding complex formation, and a Fermi contact interaction is observed. These latter specific collisional complexes are readily obtainable via DFT calculations of this interaction, providing direct comparison to the experimental results. The attitude and magnitude of weak hydrogen-bonding interactions were computationally determined for a large number of conformations for the $\text{CH}_3\text{CN}/\text{TEMPO}$ and $\text{CH}_3\text{CONH}_2/\text{TEMPO}$ systems as described below.

TEMPO: Hyperfine Couplings. As a preliminary test of the DFT computational approach, intramolecular hyperfine coupling constants were examined for the nitroxide, TEMPO. The experimental intramolecular hyperfine coupling constants based on experimental ^{13}C NMR contact shifts are reported by Hatch and Kreilick.⁶⁶ As illustrated in Table 4, calculations performed on the TEMPO molecule for the DFT geometry optimized monoclinic crystal structure⁴⁶ correlate well with the

(64) LaMar, G. *NMR of Paramagnetic Molecules: Principles and Applications*; Academic Press: New York, 1973.

(65) McConnell, H. M.; Chestnut, D. *J. Chem. Phys.* **1958**, *28*, 107–117.

(66) Hatch, G.; Kreilick, R. *J. Chem. Phys.* **1972**, *57*, 3696–3699.

Table 4. Experimental and Calculated (DFT) Hyperfine Coupling Constants (MHz)


position	experimental (MHz)	calculated (MHz)	
α	-10.1 ⁶⁶	-9.3	
β_{axial}	+13.7 ^a	+16.9	+12.2 ^b
$\beta_{\text{equatorial}}$		+7.4	
β_{ring}	+2.3	+1.7	
γ	-0.90	-0.63	
N	+45.7	+33.6	
O	-	-37.6	

^a The data assignment is based on an average of β_{axial} and $\beta_{\text{equatorial}}$, see experimentally reported data.⁶⁶ ^b Average of the calculated β_{axial} and $\beta_{\text{equatorial}}$.

experimental values reported.⁶⁶ The computational and experimental data show that the unpaired electron spin density is mainly localized on the oxygen and nitrogen atoms. As expected, the calculated coupling constants have a significantly higher value for the oxygen atom and the values decrease at increasing distances from the oxygen atom. The characteristic alternation of sign for the coupling constants proceeds around the six-membered carbon ring with the α , β , and γ carbons exhibiting -, +, and - signs, respectively.

TEMPO/Substrate Intermolecular Hyperfine Couplings.

Several different orientations of the $\text{CH}_3\text{CN}/\text{TEMPO}$ system were examined for the intermolecular interactions between CH_3CN and TEMPO, and several orientations are presented in the Supporting Information. Our first criterion for evaluating the various orientations is based on the corresponding relative energies of the intermolecular interactions, and the three orientations with the lowest total energy as a function of distance are shown in Figure 4a. The three orientations, **1**, **2**, and **3**, with the lowest energy illustrate the different attitude dependence of the $\text{N}-\text{O}\cdots\text{H}-\text{C}$ interaction. The orientations were calculated at oxygen-hydrogen distances of 0.9–4.6 Å in increments of 0.5 Å. The energy minimum occurs at 2.1 Å, which is within the range previously suggested by literature for related CH_3CN studies.^{31–33,44} All the relative energy curves indicate a distance of 2.1 Å at the minimum energy, and a range of approximately ± 0.5 Å has been arbitrarily placed on the calculated data. The lower graph provides the calculated $^{13}\text{CH}_3$ hyperfine coupling constants for the 45° orientation. As expected, based on steric repulsion arguments, the **1** [$\text{N}-\text{O}\cdots\text{H}-\text{C}$, 90°] conformation exhibits consistently higher energy at all distances relative to the other two conformations.

As previously described, the hyperfine coupling constants were experimentally measured for ^{15}N , $^{13}\text{CH}_3$, and ^{13}CN of the $\text{CH}_3\text{CN}/\text{TEMPO}$ system. It should be noted that the methyl ^1H hyperfine interaction was not experimentally accessible by the DNP technique, but these values were computed and are given in the Supporting Information. The methyl carbon has the highest hyperfine value 0.66 ± 0.04 MHz which is significantly greater than those of the cyano carbon (~ 0 MHz) or nitrogen (-0.08 ± 0.02 MHz). This hyperfine coupling constant is shown

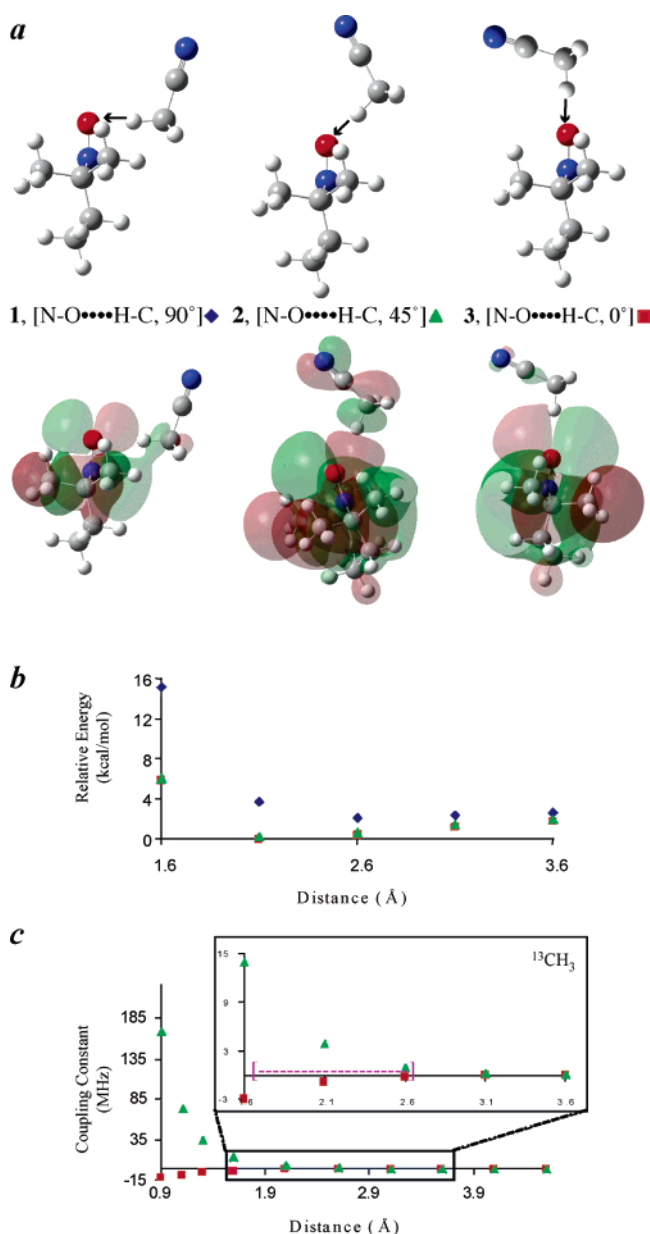


Figure 4. $\text{CH}_3\text{CN}/\text{TEMPO}$ system. (a) The three lowest-energy orientations (top) and highest occupied molecular orbital (bottom). (b) Plot of distance vs relative energy for the orientations above. (c) Plot of distance vs hyperfine coupling constant for the two orientations exhibiting the lowest relative energies (45° and 0°).

as a dashed line on the graph in Figure 4c. The large experimental hyperfine coupling constant for the methyl carbon indicates there is a stronger interaction between the methyl group of CH_3CN and the $\text{N}-\text{O}$ group of TEMPO.

The calculated hyperfine coupling constants and relative energies for each orientation are shown in Figure 4b. As illustrated, the relative energy curves for all three orientations indicate that the conformations with the lowest energy are the orientations **2** [$\text{N}-\text{O}\cdots\text{H}-\text{C}$, 45°] and **3** [$\text{N}-\text{O}\cdots\text{H}-\text{C}$, 0°]. The calculated and experimental hyperfine coupling constant results are also plotted in Figure 4c as a function of distance between the nitroxide nitrogen and the hydrogen of the methyl group ($\text{N}-\text{O}\cdots\text{H}-\text{C}$). The hyperfine coupling constant data presented in Figure 4c suggests that orientation **3** [$\text{N}-\text{O}\cdots\text{H}-\text{C}$, 0°] does not reproduce the experimental hyperfine coupling constant value for the methyl carbon. However, the computational results

suggest that orientation **2** [$\text{N}-\text{O}\cdots\text{H}-\text{C}$, 45°] reproduces the experimental data with respect to both the sign and magnitude of the experimental hyperfine coupling ($+0.66$ MHz). In addition, the negative sign calculated for the hydrogen coupling in this conformation (see Supporting Information (SI), S32) is consistent with the upfield chemical shifts previously reported for most weak hydrogen bonding in these systems.⁶⁷ However, earlier work by Morishima and co-workers for the di-*tert*-butyl nitroxide/ CH_3CN system suggest an ^1H NMR contact for the methyl hydrogens that is nearly zero.⁶⁷

The agreement of the $^{13}\text{CH}_3$ experimental data for the conformation **2** could be due to a combination of steric repulsive factors and optimized transfer of spin density to the carbon nucleus. One might predict that the best spin density transfer would occur at the 90° orthogonal orientation **1**, where the methyl hydrogen interacts directly with the π -orbital of the TEMPO oxygen; however, steric repulsive interactions between the methyl hydrogen atoms of CH_3CN and methyl hydrogen atoms of TEMPO appear to diminish the importance of this conformation. This is also apparent from the HOMO diagram (Figure 4a) for the three orientations as well as the poor agreement for the calculated hyperfine sign for both the hydrogen and carbon of the CH_3 group of the CH_3CN . Figure 4a illustrates the HOMO molecular orbital diagrams for the different orientations which clearly show significantly better orbital overlap for **2** [$\text{N}-\text{O}\cdots\text{H}-\text{C}$, 45°] conformation with good agreement of the magnitude and sign of the hyperfine coupling. Therefore, the **2** [$\text{N}-\text{O}\cdots\text{H}-\text{C}$, 45°] orientation (Figure 4a, middle) appears to be consistent with the various factors influencing weak hydrogen-bonding interactions. Although the approach described above did not include the influence of solvent or other solute molecules (CH_3CN), we did examine the influence of solvent (CCl_4) using the polarizable continuum model (PCM, Gaussian 3) for orientation **2**. The PCM results for $\text{CH}_3\text{CN}/\text{TEMPO}$ with orientation **2** provide only very minor changes in the computed magnitude values for the calculated hyperfine couplings (see SI). We also examined the influence of the electronegative group in the substrate molecule by changing from the $\text{CH}_3\text{CN}/\text{TEMPO}$ to the $\text{CH}_3\text{-CH}_3/\text{TEMPO}$ system and repeating the same calculations described above in Figure 4 (see SI). Surprisingly, the results for the $\text{CH}_3\text{CH}_3/\text{TEMPO}$ conformations for **1–3** at the same orientations and distances were very similar to the $\text{CH}_3\text{CN}/\text{TEMPO}$ system at the B3LYP level. Since it is well recognized that molecules with methyl groups and other sp^3 -hybridized nonacidic carbons ($\text{N}-\text{O}\cdots\text{H}-\text{C}$) not adjacent to electronegative groups usually exhibit very reduced scalar interactions usually dominated by only dipolar interactions with nitroxides.^{23,24,27,55} These results suggest that the intermolecular hyperfine interaction (a) is mainly influenced by “close-in” spin interactions in the transient [$\text{N}-\text{O}\cdots\text{H}-\text{C}$] complex. In addition, the electronegative group (e.g., cyano group) in intermolecular $\text{CH}_3\text{-CN}/\text{TEMPO}$ solution collisions provides longer lifetimes that yield dominant scalar interactions for weak hydrogen-bonding interactions. As noted above, the experimentally derived scalar interaction-derived value of ~ 85 ps estimated for the $\text{CH}_3\text{CN}/\text{TEMPO}$ system is 2–3 times longer than the rotational correlation time. In summary, the computational results for

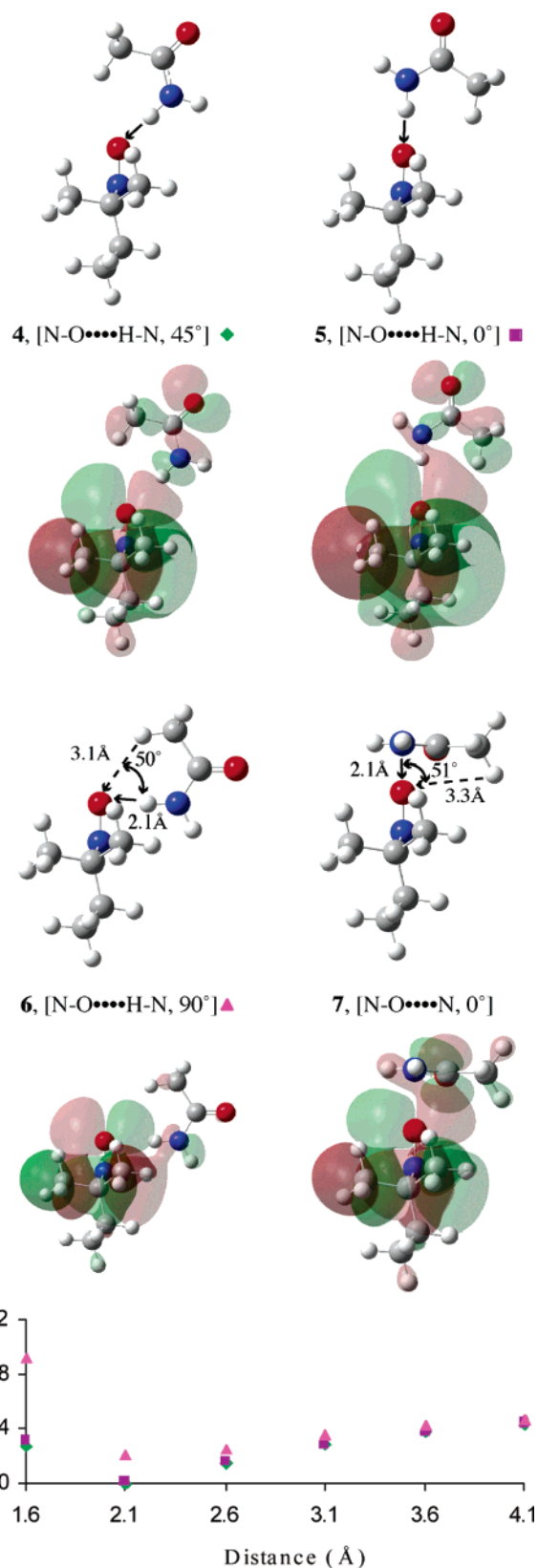


Figure 5. $\text{CH}_3\text{CONH}_2/\text{TEMPO}$ favored orientations (top) and highest occupied molecular orbital for each favored orientation (bottom). Plot of distance vs hyperfine coupling constant for three orientations.

orientation **2** [$\text{N}-\text{O}\cdots\text{H}-\text{C}$, 45°] are consistent with the experimental hyperfine data of TEMPO and clearly illustrate weak carbon–hydrogen bonding of the nitroxide with the methyl group of CH_3CN .

(67) Morishima, I.; Matsui, T.; Yonezawa, T.; Goto, K. *J. Chem. Soc., Perkin Trans. 2* **1972**, 633–635.

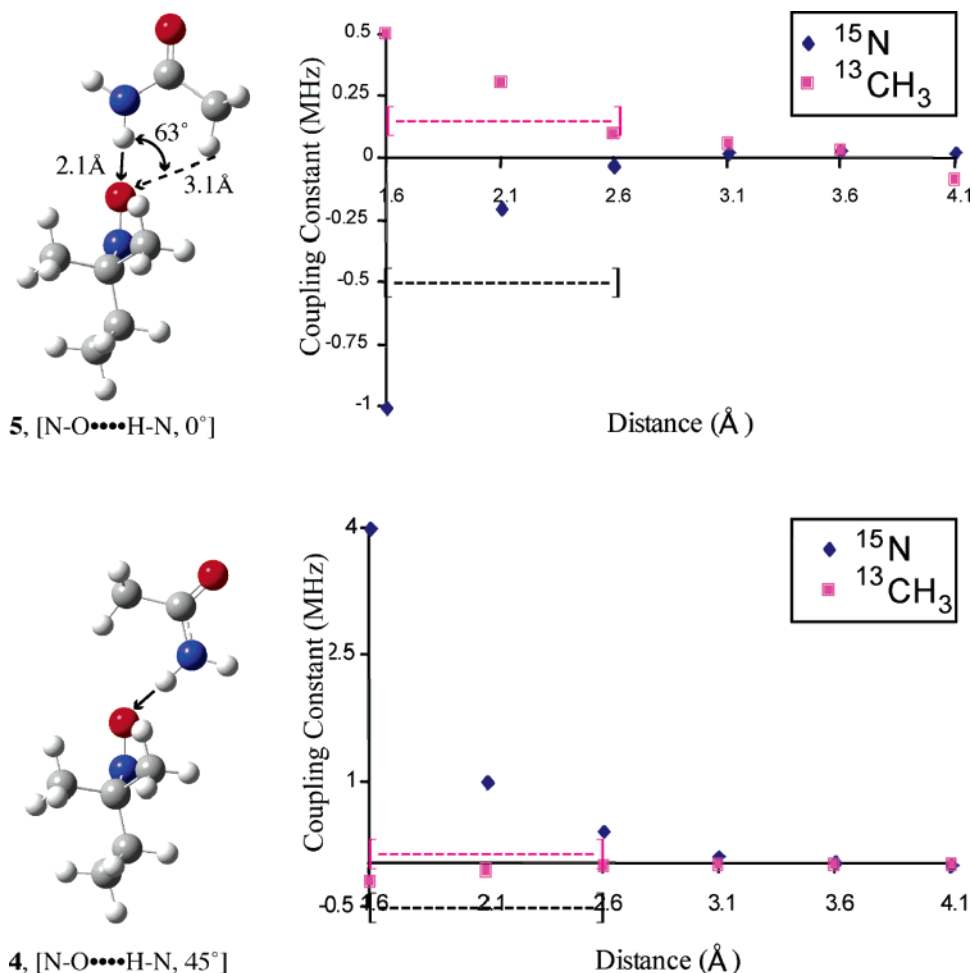


Figure 6. CH₃CONH₂/TEMPO system. Calculated and experimental hyperfine coupling constants vs distance.

For the CH₃CONH₂/TEMPO system, 13 orientations were calculated to ascertain the site, attitude, and distance of the optimized hyperfine interactions between CH₃CONH₂ and TEMPO. Three of the orientations illustrated in Figure 5 represent the lowest-energy orientations examined **5–7** and orientations **4–7** represent those conformations that agree with the experimental (–) and (+) sign respectively, for the amide nitrogen ($a/h = -0.55$ MHz) and methyl carbon ($a/h = 0.18$ MHz). Several alternative orientations are presented in the Supporting Information. Furthermore, the computational results show that the –NH₂ group of CH₃CONH₂ is sp²-hybridized and planar, as illustrated in Figure 5. The crystal structure of CH₃CONH₂ determined by Senti et al.⁶⁸ is in agreement with the planar structure calculated, and the Cartesian coordinates for the geometry optimized CH₃CONH₂ molecule are provided in the Supporting Information. For orientations **4–6**, the relative energy minimum occurs at 2.1 Å, in similar fashion to the distance obtained for the CH₃CN/TEMPO system. Orientation **7** in Figure 5 shows the [N–O...N] interaction and has a higher minimum energy than the other three conformations but is an orientation conformation that reproduces the experimental hyperfine coupling constant data for the amide nitrogen and methyl carbon. In this case, the π -orbital of the CH₃CONH₂ nitrogen presumably interacts with the s-orbital of TEMPO

oxygen. Additional data for this orientation is summarized in the Supporting Information.

As previously indicated (Table 3), the nitrogen nuclide exhibits the greater absolute hyperfine value of -0.5 ± 0.04 MHz compared to the methyl carbon (0.16 ± 0.01 MHz), and both are significantly greater than the carbonyl carbon (-0.01 ± 0.02 MHz). As expected, the significantly larger hyperfine value at the nitrogen nucleus indicates a stronger interaction between the amide and the NO group for TEMPO when compared with the other two possible interaction sites (e.g., carbonyl and methyl groups). However, a significant competition between the amide (–NH₂) and methyl (–CH₃) sites is also suggested.

Of the four orientations presented in Figure 5, the orientational conformations **4** [N–O...H–N, 45°] and **5** [N–O...H–N, 0°] have the lowest relative energy. The calculated and experimental hyperfine coupling constants for the ¹⁵N- and ¹³CH₃-acetamide nuclei for these orientations are presented in Figure 6. The lower graph shows that the data for the **4** [N–O...H–N, 45°] orientation clearly illustrate the poor agreement of the experimental hyperfine coupling constants with the computational values. In contrast, the upper graph in Figure 6 illustrates data for the **5** [N–O...H–N, 0°] orientation which provide good agreement between the experimental hyperfine coupling constants both in terms of the sign and magnitude for both the ¹³CH₃ and ¹⁵NH₂ nuclei, $a/h = 0.16$ and -0.50 MHz, respec-

(68) Senti, F.; Harker, D. *J. Am. Chem. Soc.* **1940**, *62*, 2008–2019.

tively. Thus, we suggest that the **5** [N–O···H–N, $\theta = 0^\circ$] orientation is one of the more important contributions for the CH₃CONH₂/TEMPO intermolecular interaction. However, it should be noted that a number of different conformations (or combinations) could be important in describing this weak hydrogen-bonding interaction especially for a molecule with more than one interaction site. In this regard, the [N–O···H–C, 45°] orientation that was favored for the previously described CH₃CN/TEMPO system also exhibits good agreement for the sign and magnitude of the –CH₃ carbon, but not the –NH₂ nitrogen (see SI). The difference in the attitude between the C–H bond of the –CH₃ group in both systems and the N–H bond in the CH₃CONH₂/TEMPO system [N–O···H–C, 45°] and [N–O···H–N, 0°], respectively, could be a result of the changed hybridization of a methyl group (sp³) vs an amide group (sp²).

Conclusions

In summary, weak hydrogen bonding and a corresponding hyperfine interaction is observed at relatively acidic H–C or H–N sites in the substrate molecules CH₃CN and CH₃CONH₂. The attitude of the interaction critically defines the magnitude and sign of the corresponding hyperfine interaction. For example, the straight-on orientation for the amine group of CH₃CONH₂ **5** [N–O···H–N, 0°] and the 45° orientation for the methyl of the CH₃CN/TEMPO **2** are found to be important conformations for significant scalar interactions. The DFT values computed for conformation **5** [N–O···H–N, $\theta = 0^\circ$] for the CH₃CONH₂/TEMPO system provides good agreement for the CH₃CONH₂/TEMPO interaction with the experimental hyperfine coupling constants and suggests an important interaction with the –NH₂ group of the CH₃CONH₂ molecule during collisions in solution. This orientation suggests a decrease in the steric repulsions in comparison with other orientations. The **5** [N–O···H–N, $\theta = 0^\circ$] orientational confirmation also exhibits

methyl hydrogens at a 63° angle with respect to the TEMPO oxygen (Figure 6). The 63° angle compares favorably with the 45° orientation also found for the CH₃CN methyl–hydrogen interaction. The results of this study also suggest that the intermolecular hyperfine interaction (*a*) is mainly influenced by “close-in” interactions in the transient substrate/nitroxide complex that are not significantly influenced by the solvent as based on PCM computational results. The preferred conformations (e.g., **2** for CH₃CN/TEMPO) suggest longer scalar lifetimes that yield dominant scalar interactions for these weak hydrogen-bonding interactions. In conclusion, a major finding of this study is that solution intermolecular scalar interactions can be accurately modeled at the UB3LYP level in terms of the magnitude and attitude for substrate/nitroxide complexes.

Acknowledgment. Dedicated to the memory of over thirty students and faculty who lost their lives on April 16, 2007 at Virginia Tech. We gratefully acknowledge financial support for this work from the National Science Foundation, Westvaco Company, Eastman Kodak Company, and the Petroleum Research Foundation. J.C.D. acknowledges the support of an Appalachian College Association John B. Stephenson Fellowship.

Supporting Information Available: Complete refs 47 and 48 (p S2), computational details (p S3), Cartesian coordinates for TEMPO, etc. (p S6), calculated conformations, energies, etc. for the acetonitrile/TEMPO system (p S11), calculated conformations, energies, etc. for the acetamide/TEMPO system (p S20), and the computed hydrogen Fermi contact coupling constants (p S32) are available as Supporting Information. This material is available free of charge via the Internet at <http://pubs.acs.org>.

JA064632I